Marine CO_2 system variability in a high Arctic tidewater-glacier fjord system, Tempelfjorden, Svalbard

Ylva Ericson[1, 2], Eva Falck[1, 2], Melissa Chierici[1, 3], Agneta Fransson[4], and Svein Kristiansen[5]

[1]Department of Arctic Geophysics, University Centre in Svalbard, P.O. Box 156, N-9171 Longyearbyen, Norway.

[2]Geophysical Institute, University of Bergen, Allégaten 70, 5007 Bergen, Norway.

[3]Institute of Marine Research, Fram Centre, Hjalmar Johansens gate 14, 9007 Tromsø, Norway.

[4]Norwegian Polar Institute, Fram Centre, 9296 Tromsø, Norway.

[5]Department of Arctic and Marine Biology, UiT The Arctic University of Norway, PO Box 6050 Langnes, 9037 Tromsø, Norway.

Corresponding author: Ylva Ericson, University Centre in Svalbard, P.O. Box 156, N-9171 Longyearbyen, Norway, ylva.ericson@unis.no

Declarations of interest: none.

Keywords: marine CO_2 system, pCO_2, aragonite, freshwater, Arctic fjord, Svalbard

Abstract

The marine CO_2 system in Tempelfjorden (Svalbard) was investigated between August 2015 and December 2017 using total alkalinity, pH, temperature, salinity, oxygen isotopic ratio, and nutrient data. Primary production resulted in the largest changes that were observed in the partial pressure of CO_2 (pCO_2, 140 µatm) and the saturation state of aragonite (Ω_{Ar}, 0.9). Over the period of peak freshwater discharge (June to August), the freshwater addition and air-sea CO_2 uptake (on average 15.5 mmol m^{-2} day^{-1} in 2017) governed the surface pCO_2. About one fourth of the uptake was driven by the freshening. The sensitivity of Ω_{Ar} to the freshwater addition was investigated using robust regressions. If the effect of air-sea CO_2 exchange was removed from Ω_{Ar}, a freshwater fraction larger than 50% (lower range of uncertainty) was needed to provide aragonite undersaturated waters. This study shows that Ω_{Ar} and freshwater fraction relationships that are derived from regression techniques and the interpretation thereof are sensitive to the effect of air-sea CO_2 exchange. Since the freshening in itself only drives a fraction of the air-sea CO_2 uptake, studies that do not account for this exchange will overestimate the impact of freshwater on Ω_{Ar}. Finally, in the summer an excess in the salinity normalized dissolved inorganic carbon, corrected for aerobic primary production/respiration, of on average 86 µmol kg^{-1} was found in the deepest water of the fjord. This excess is suggested to be a result of enhanced CO_2 uptake and brine release during the period of sea ice growth.

1. Introduction

Knowledge of the carbon cycling in Arctic coastal systems is of great importance as these areas, apart from contributing with roughly one fourth of the global coastal ocean (i.e. shallower than 200 m, Menard and Smith, 1966), are among the first to respond to climate change due to the Arctic amplification (Serreze and Francis, 2006). Recent studies have focused on glacier-influenced fjord environments where glacial meltwater has been proposed to contribute significantly to the observed low partial pressure of CO_2 (pCO_2) of the surface water and subsequently the high CO_2 uptake of the fjords (e.g. Rysgaard et al., 2012; Meire et al., 2015), but glacial meltwater may affect the marine CO_2 system in other ways as well. For instance, lower saturation state (Ω) of the calcium carbonate ($CaCO_3$) mineral aragonite (Ω_{Ar}) has been coupled to high glacial meltwater content as compared to the correspondent Ω_{Ar} of seawater (e.g. Fransson et al., 2015), which is of relevance for ongoing Ocean Acidification (OA). OA refers to the combined effects of the oceanic uptake of anthropogenic CO_2, which results in shifts in the equilibria of the seawater acid-base systems (Doney et al., 2009). Changes in the chemical speciation of the marine CO_2 system due to the dissolution of anthropogenic CO_2 has resulted in a lower oceanic pH

(i.e. a decrease of about 0.1 units since pre-industrial times, Rhein et al., 2013), as well as in a reduced carbonate ion concentration ($[CO_3^{2-}]$). The latter determines Ω according to the following:

$$\Omega = \frac{[CO_3^{2-}][Ca^{2+}]}{K_{sp}^*} \quad (1)$$

where $[Ca^{2+}]$ is the calcium ion concentration and K_{sp}^* is the stoichiometric solubility product for water that is saturated in $CaCO_3$. For Ω less than 1, $CaCO_3$ may dissolve, which is of importance for calcifying marine organisms that have their biotic $CaCO_3$ shells exposed to the surrounding seawater. Ω is thus an excellent indicator of marine systems sensitivity to OA, and its relation to freshwater can be used to predict the future Ω of Arctic surface waters. For instance, Turk et al. (2016) showed for the estuary Cumberland Sound in the Canadian Archipelago that a fraction of river runoff and glacial meltwater larger than 37% results in aragonite undersaturated waters, but the effect of air-sea CO_2 exchange was not accounted for. Evans et al. (2014) on the other hand, argued for the glacial melt influenced region of Prince William Sound, Alaska, that it is rather the cumulative effects of glacial melt and CO_2 uptake that reduce Ω.

Glacial melt may also have both negative and positive impacts on primary production (e.g. Arrigo et al., 2017; Lund-Hansen et al., 2018), which is one of the key drivers of Ω_{Ar} in the West Spitsbergen fjords (Fransson et al., 2016; Ericson et al., submitted to Polar Research). Observations of glacier retreats in this area are accumulating (e.g. Ziaja 2005; Ewertowski, 2014; Marlin et al., 2017; Grabiec et al., 2017), and more freshwater is thereby being released to the surrounding fjord systems. At the same time, the sea ice cover has decreased (e.g. from 60 to 20% between 2000-2005 and 2006-2014 in Isfjorden, Muckenhuber et al., 2016), which has been attributed to increased intrusions of Atlantic Water (AW, S > 34.9) (Nilsen et al., 2016), that also has become warmer (0.2°C/decade in Isfjorden, Pavlov et al., 2013). AW is carried by the West Spitsbergen Current (WSC) that follows the continental slope towards the entrance of the central Arctic Ocean. Apart from this rather warm and saline water mass, the fjords are influenced by cold Arctic Water (ArW, S < 34.7) that flows northwards along the coast with the Coastal Current (CC, e.g. Cottier et al., 2005; Nilsen et al., 2008). Some of the AW that enters the fjords is modified through mixing with the ArW on the shelf. This freshened and slightly colder water mass is referred to as Transformed Atlantic Water (TAW, 34.7 < S < 34.9).

Tempelfjorden (Fig. 1), on the West Spitsbergen coast, is the easternmost fjord branch of the Isfjorden system. It has two basins, one deeper (110 m), more central basin that extends well into the connecting Sassenfjorden, and one smaller basin closer to the tidewater-glacier Tunabreen and the land-terminating glacier von Postbreen, at the head of the fjord (Forwick et al., 2010). The glaciers provide Tempelfjorden with freshwater and sediments with carbonate (ankerite/dolomite and calcite) and silicate (epidote and phyllosillicates) rich minerals (Forwick et al., 2010). The river Sassenelva, located outside

the entrance of the fjord, is also an important freshwater source that brings sediments with mainly silicate rich minerals (e.g. phyllosillicates) (Forwick et al., 2010). Tempelfjorden has been investigated previously by Fransson et al. (2015) who showed that released freshwater decreased Ω, pH, and total alkalinity (TA). On the other hand, the addition of calcareous minerals from the bedrock to the fjord water increased the TA relative to salinity and partly mitigated the effect of freshwater on the marine CO_2 system (Fransson et al., 2015). Tunabreen is a surging glacier, with a return period of about 40 years (Forwick et al., 2010). The last documented surge occurred between 2003 and 2005 (Forwick et al., 2010), but recent advances of the glacier front over the last couple of years have become referred to as a surge despite the unexpectedly short return time of a little more than a decade or so. The frequent calving of the glacier provides a unique opportunity to study how glacier melt affects the marine CO_2 system throughout the year on a higher resolution than has been seen previously in this fjord. Since the fast sea ice cover has diminished in the region, this study will also give insights to marine CO_2 system dynamics in a potential future with less sea ice.

Here we present measured pH and TA data from Tempelfjorden with related calculated marine CO_2 system parameters observed between the end of August 2015 and early December 2017. The time series of the measured and calculated parameters are shown in Section 3 while Section 4 will concentrate on the period of meltwater input (June-August) where the effects of freshwater on the marine CO_2 system will be discussed in the light of potential increased meltwater discharges in the future with a focus on Ω_{Ar}.

Some emphasis will be put on the sensitivity of regression-based methods to air-sea CO_2 exchange. Also, CO_2-enriched bottom water will be discussed considering a reduced future sea ice production.

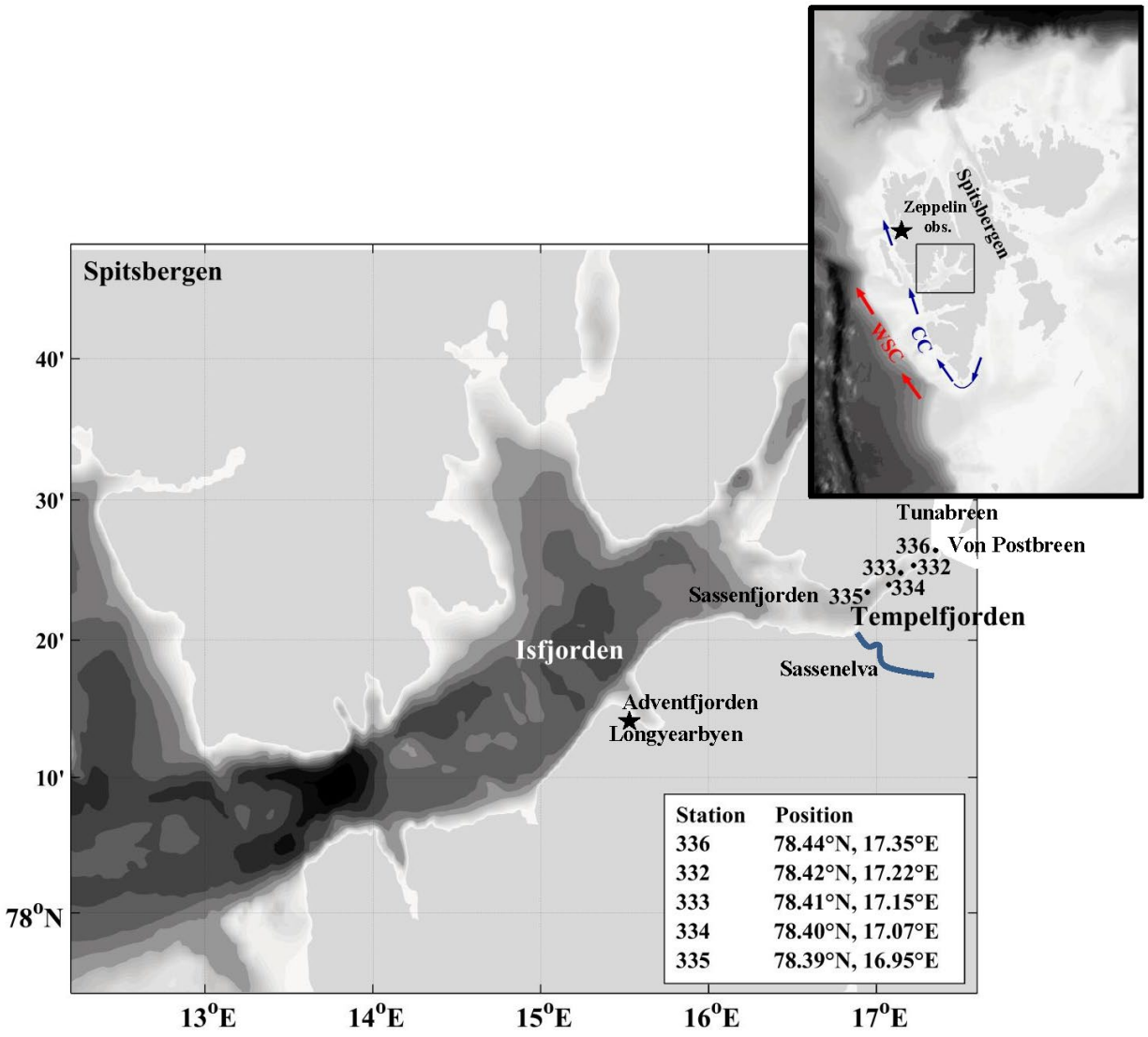

Fig. 1. Map of Svalbard, including the West Spitsbergen Current (WSC, red arrows) and the Coastal Current (CC, blue arrows), with outcrop of Isfjorden on the west coast of Spitsbergen showing the station locations in Tempelfjorden.

2. Materials and Methods

Seawater was collected, typically from a small boat, between 29 August 2015 and 5 December 2017 (Table 1). The sampling frequency was initially every other month in autumn 2015, monthly in 2016, and after a long break between January and June in 2017 close to monthly. The following properties were collected: pH/TA, oxygen isotopic ratio ($\delta^{18}O$), and nutrients (i.e. the concentrations of nitrate, $[NO_3^-]$, and silicic acid, $[Si(OH)_4]$). Water column temperature and salinity were measured using

conductivity-temperature-depth (CTD) sensors (i.e. using one of the following devices depending on sampling occasion according to Table 1: SAIV A/S SD204 CTD, Sea-Bird SBE9/SBE37/SBE19+). The most frequent profiler used was the SBE19+ which was calibrated each year and deployed together with the SD204 or the SBE37 on a few occasions to cross-check the performances of the individual sensors.

Table 1

Data Overview

Dates	CTD	Stations	Bottom depths (m)	Max sampling depths (m)	TA/pH	$\delta^{18}O$	Nutrients
29 Aug 2015	SBE9	336, 332, 333, 334, 335	41, 28, 77, 88, 101	33, 21, 70, 85, 96	Yes[a]	No	No
27 Oct 2015	SBE37	336, 332, 333, 334, 335	41, 35, 74, 87, 105	35, 25, 71, 80, 91	Yes	Yes	Yes
2 Dec 2015	SBE37	336, 332, 333, 334, 335	51, 34, 76, 91, 104	45, 25, 70, 81, 90	Yes	Yes	Yes
29 Jan 2016	SBE37	336, 333, 335	47, 72, 104	39, 24, 49	Yes	Yes	Yes
19 Feb 2016	SBE19+	336[b], 332, 333, 334, 335	47, 35, 70, 92, 105	40, 26, 50, 77, 85	Yes	Yes	Yes
4 Mar 2016	SBE19+	336, 332, 333, 334, 335	42, 37, 75, 91, 104	33, 27, 65, 83, 98	Yes	Yes	Yes
29 Mar 2016	SBE19+	333, 334, 335	80, 89, 104	65, 75, 87	Yes	Yes	Yes
29 Apr 2016	SBE19+	335	104	91	Yes	Yes	Yes
3 May 2016	SBE19+	335	104	85	Yes	Yes	Yes
20 May 2016	SBE19+	336[c], 333, 335	36, 78, 105	23, 68, 89	Yes	Yes	Yes
1 Jun 2016	SBE19+	336, 333, 335	49, 83, 104	39, 68, 88	Yes	Yes	Yes
20 Jun 2016	SBE19+	336, 333, 335	45, 78, 104	30, 65, 81	Yes	Yes	Yes
4 Jul 2016	SBE19+	336, 333, 335	42, 75, 103	35, 70, 90	Yes	Yes	Yes
1 Aug 2016	SBE19+	336, 333, 335	46, 82, 99	45,70,87	Yes	Yes	Yes
20 Sep 2016	SD204[d]	336, 333, 335	45, 76, 105	41, 70, 84	Yes	Yes	Yes
11 Oct 2016	SBE19+	336[e], 333, 335	39, 74, 104	35, 71, 90	Yes	Yes	Yes
1 Nov 2016	SBE19+	332, 333, 335	32, 74, 102	25, 68, 92	Yes	n/a[f]	Yes
16 Dec 2016	SBE19+	335	103	91	Yes	n/a[f]	Yes
16 Jun 2017	SBE19+	336, 333, 335	45, 76, 105	35, 65, 94	Yes	n/a[f]	Yes
20 Jul 2017	SBE19+	336, 333, 335	40,78, 105	36, 68, 86	Yes	n/a[f]	Yes
1 Aug 2017	SBE19+	336[g], 333, 335	36, 74, 103	25, 65, 89	Yes	n/a[f]	Yes
31 Aug 2017	SBE19+	336, 333, 335	40, 78, 105	40, 64, 89	Yes	n/a[f]	Yes
30 Sep 2017	SBE9	336[h], 332, 333, 334, 335	40, 43, 72, 90, 101	30, 28, 62, 79, 92	Yes	n/a[f]	Yes

7 Nov 2017	n/a[i]	336, 333, 335	39, 80, 100	25, 65, 90	Yes	n/a[f]	Yes
5 Dec 2017	SBE19+	336, 333, 335	41, 76, 102	25, 65, 90	Yes	n/a[f]	Yes

Note. [a]Fixated with $HgCl_2$ and analysed within 6 weeks. [b]Position altered to 78.43°N and 17.32°E due to sea ice. [c]Position altered to 78.43°N and 17.30°E due to sea ice. [d]Noise in pressure measurements i.e. pressure was modelled, salinity recalculated for the new pressure, and finally, salinity was corrected for an offset of -0.13. [e]Position altered to 78.43°N and 17.26°E due to glacier ice. [f]Pending analysis. [g]Position altered to 78.43°N and 17.29°E due to glacier ice. [h]Same position as 1 Aug 2017 i.e. 78.43°N and 17.29°E. [i]CTD-measurements failed, water sample salinity was measured using a Portasal 8410A salinometer and was calibrated against IAPSO standard sea water, OSIL Environmental Instruments and Systems, batch: P146. Temperature was interpolated from the measurements of the previous and the following sampling occasion.

The pH/TA samples were typically analysed the same day as the sampling took place or the day after. TA was determined using a non-linear least square optimisation (DOE, 1994) of potentiometric titration data from a non-purged open cell (Metrohm© Titrando system, Switzerland) with a precision around ± 2.3 µmol kg^{-1} (i.e. the mean of all absolute valued differences between duplicate sample runs). In April 2016 the non-linear least square calculation failed for four of the samples and an optimized end-point determination was used instead (Metrohm© tiamo™ - titration software, Switzerland). The precision of this method is typically about ± 4 µmol kg^{-1} and the two methods differ in average by 2 µmol kg^{-1}. All samples were calibrated against Certified Reference Materials (CRM, purchased from A. Dickson, Scripps Institution of Oceanography, USA), and the resultant accuracy should be in the order of the precision. This was confirmed by an inter-laboratory comparison in May 2017 (organized by the laboratory of A. Dickson, Scripps Institution of Oceanography, USA) where the measured TA of both methods differed by less than 1 µmol kg^{-1} from the certified TA values of the CO_2 Inter-laboratory comparison samples. pH was measured spectrophotometrically according to Clayton and Byrne (1993) using the dye *m*-cresol purple (*m*CP), with a precision around ± 0.001. This method gives pH on the total pH scale (pH_T). The correction of Chierici et al. (1999) was used to remove the effect of the indicator pH on the sample pH. The accuracy of the pH is likely in the order of ± 0.005 as indicated by the inter-laboratory comparison where for ambient pCO_2 conditions the measured pH was 0.005±0.001 higher than the certified value. Note that two batches of non-purified *m*CP were used over the study and both were tested during the inter-laboratory comparison.

The $\delta^{18}O$ samples were stored cold (4°C) and analysed within roughly one year at the Geological Mass Spectrometry (GMS) laboratory at the Department for Earth Science, University of Bergen,

Norway. The GMS laboratory uses a Thermo Finnigan Delta V with a Gasbench which is calibrated against VSMOW II.

The nutrients samples were immediately frozen after each sampling occasion and stored in the dark until analysis that took place within less than one year. The nutrient samples that were collected from October 2015 until May 2016 were sent to the Institute of Marine Research, Bergen, Norway, for analysis (Alpkem Flow Solution IV or Skalar autoanalyzers) using methods according to Bendschneider and Robinson 1952 (the RFA methodology) and Grasshof 1965 for [NO_3^-] and [$Si(OH)_4$], respectively, with the correspondent detection limits of 0.4 and 0.7 μmol kg^{-1}, respectively. Samples that were collected between June and August 2017 were analysed using a Flow Solution IV analyser, O.I. Analytical, USA, at UiT-The Arctic University of Norway, Tromsø, Norway, with methods adapted from Grasshof et al. (2009). The detection limits were 0.04 and 0.07 μmol kg^{-1} for [NO_3^-] and [$Si(OH)_4$], respectively. The remaining nutrient samples were analysed at the University Centre in Svalbard (UNIS), Longyearbyen, Norway, using a QuAAtro autoanalyzer from SEAL Analytical with methods according to NIOZ – Royal Netherlands Institute for Sea Research, Den Hoorn, The Netherlands. Here the detection limits were 0.05 and 0.04 μmol kg^{-1}, the precisions were ±0.08 and ±0.07 μmol kg^{-1}, and the accuracies (i.e. accuracy was estimated from solutions of high-purity salts that were prepared for each day of analysis) were in the order of ± 2-3% or less for [NO_3^-] and [$Si(OH)_4$], respectively. The nutrient data were converted to μmol kg^{-1} using the density, which was calculated from a pressure of 1 atm, the sample salinity and a laboratory temperature measured at UNIS of 21°C. The temperature was assumed to be comparable between laboratories.

Related marine CO_2 system parameters (total dissolved inorganic carbon (DIC), pCO_2, the Revelle Factor $((\partial pCO_2/\partial DIC)/(pCO_2/DIC))$, and Ω_{Ar}) were computed using TA and pH, with the pressure, salinity, and temperature data as input parameters in the chemical speciation software CO2SYS (van Heuven et al., 2011). At least two recent Arctic studies (Chen et al., 2015; Woosley et al., 2017) have shown promising internal consistency for marine CO_2 system data when the carbonate stoichiometric dissociation constants (K_1* and K_2*) of Mehrbach et al. (1973) as refit by Dickson and Millero (1987) have been used. For that reason, this set of constants was used in all CO2SYS calculations in the present study as well, together with the dissociation constant of bisulphate (K_{SO4}) of Dickson (1990) and total borate as determined by the formula of Lee et al. (2010). The K_{sp}*of Mucci (1983) was used together with the pressure correction of Millero (1979). The salinity-[Ca^{2+}] relationship of Riley and Tongudai (1967) was also used. Uncertainties in the calculated properties due to uncertainties in the input parameters should be around ±7 μmol kg^{-1}, ±11 μatm, ±0.02, and ±0.07, for DIC, pCO_2, the Revelle

Factor, and Ω_{Ar} as estimated by Ericson et al. (submitted to Polar Research) for marine CO_2 system data from the neighbouring fjord branch, Adventfjorden.

To obtain a background understanding of the sea ice/glacial ice characteristics of the fjord over the study period, the ice cover was approximated from weekday ice charts of the Ice Service of the Norwegian Meteorological Institute (MET, http://polarview.met.no/) by counting pixels according to the ice chart colour scheme for very open drift ice (1-4/10ths), open drift ice (4-7/10ths), close drift ice (7-10/10ths) and fast ice (10/10ths). Note that the detected ice cover (Fig.2a) in summer and autumn typically reflects calved glacier ice from Tunabreen as observed visually. There was altogether more ice coverage in 2017 as compared to 2016 (Fig. 2c-f). By the end of March in 2017 the fast sea ice covered the whole fjord, including most of the connecting fjord, Sassenfjorden (own observation), which can be compared to 2016 when the fast sea ice never reached beyond about 50% coverage (Fig. 2c). In total, there were around 50 weekdays when the ice cover irrespective of openness was 75% or larger of which roughly 20 and 30 of the weekdays occurred in 2016 and 2017, respectively. This suggests that the major part of the surface water was available for air-sea CO_2 gas exchange throughout the year. Note that the calving of glacier ice in summer to autumn of 2017, as shown as very open drift ice, exceeds that of the

two previous years (Figs. 2b, d and f), which supports an increased activity of Tunabreen over the study period.

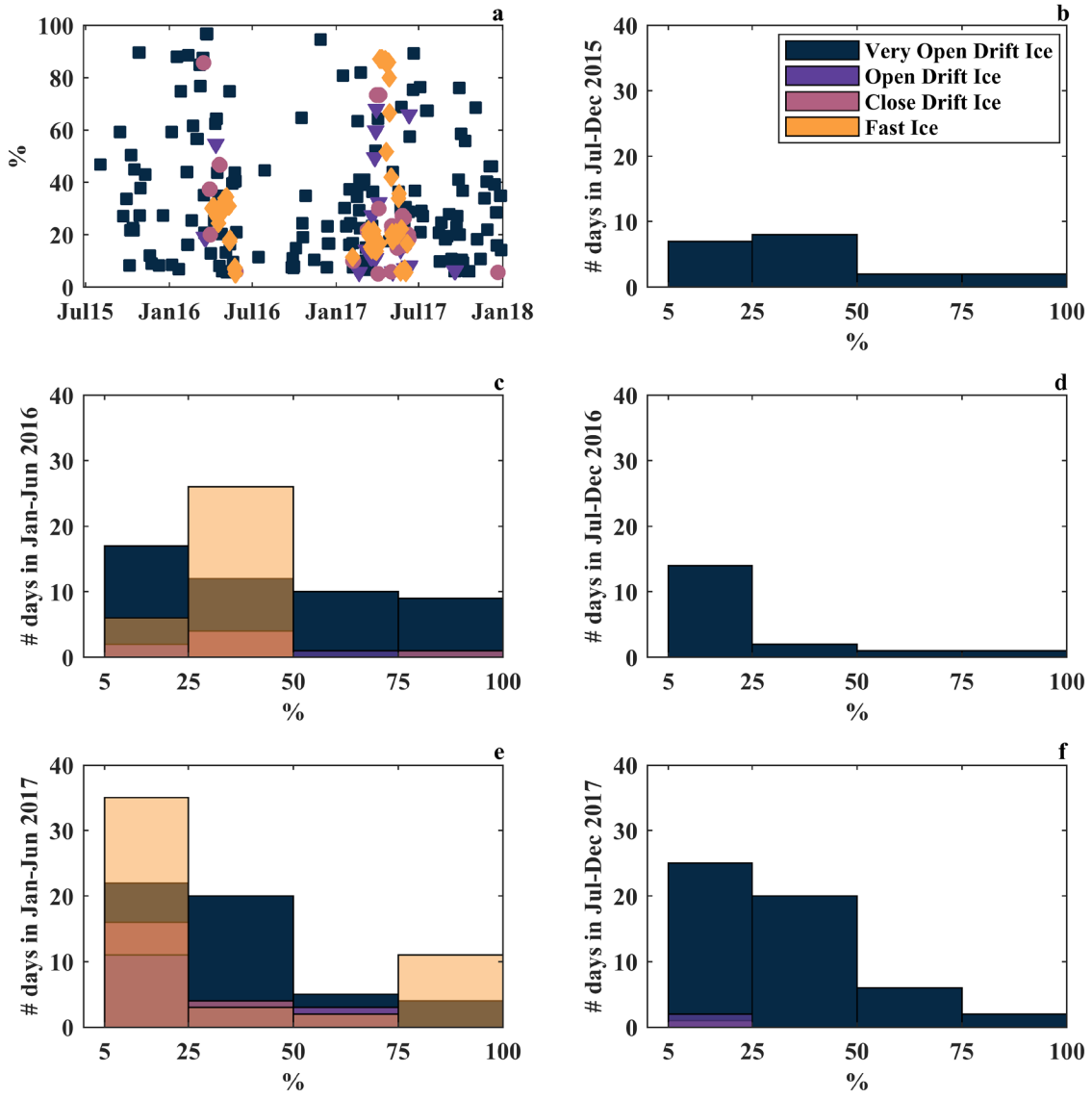

Fig. 2. Weekday ice cover (> 5%) in Tempelfjorden is shown in terms of a) Ice cover (%), and number of days with ice cover in b) July to December 2015, c) in January to June 2016, d) in July to December 2016, e) in January to June 2017, f) in July to December 2017. Colouring scheme is for very open drift ice (1-4/10ths, charcoal), open drift ice (4-7/10ths, midnight blue), close drift ice (7-10/10ths, heather) and fast ice (10/10ths, orange). Note that this is

an approximation of the ice cover as estimated from the ice charts for the Svalbard region provided by the Ice Service of the Norwegian Meteorological Institute.

To evaluate the effects of freshwater on the marine CO_2 system and associated properties, the freshwater fraction (f_{fw}) was estimated using a reference salinity of 34.8 (S_{ref}, a typical value for TAW and the highest observed salinity over the study period):

$$f_{fw} = \frac{(S_{ref} - S)}{S_{ref}} \quad (2)$$

where S is the measured salinity. If the winter (December to March) mean salinity of 34.5 would have been used as the reference salinity the freshwater fraction would be 0.9% lower. Then robust regressions were used to determine the relationships between the dependent variables (TA, DIC, and Ω_{Ar}) and the freshwater fraction for the summers of 2016 and 2017. The robust regression method was chosen over the typical linear least square calculation to reduce the influence of potential outliers. The aim of these calculations was to determine the end-member TA and DIC values of the local freshwater source and to evaluate the effect of freshwater on TA, DIC, and Ω_{Ar}. Only data from the upper 30 m of the water column were used to minimize the potential effect of bottom waters on the estimates. Also, only the period between the onset of the melt season in June and the beginning of August, when the freshwater fraction reaches its maximum (this period will be referred to as the melt season in the rest of the paper) was considered. This period was chosen to minimize the potential effect of mixing that increases with the wind intensity, which in turn increases towards the autumn as observed at the nearby located Longyearbyen airport (Ericson et al., 2018).

It has been shown that the freshening of the surface layer in the neighbouring fjord branch, Adventfjorden, occurs when the air-sea pCO_2 gradient is at its maximum after the spring bloom (Ericson et al. 2018). While the wind intensity typically is less in the summer, for instance such as observed in the vicinity of Adventfjorden (Ericson et al., 2018), the CO_2 uptake capacity is large. Regression based relationships between freshwater and the marine CO_2 system properties are for that reason likely to be biased by air-sea CO_2 exchange, especially since the freshest water resides in the surface and therefore is more affected by potential CO_2 uptake compared to the more saline water deeper down. TA versus DIC plots are commonly used to differentiate between the most important processes (e.g. biological processes, air-sea CO_2 exchange, conservative mixing, and $CaCO_3$ production/dissolution) that drive the variability in TA and DIC. These plots cannot, however, be used to differentiate between the effect of air-sea CO_2

exchange and the effect of DIC added through freshwater, unless the freshwater source DIC end-member is known.

To account for the effects of oceanic CO_2 uptake, during the melt season, on the marine CO_2 system, the air-sea CO_2 flux ($F_{air\text{-}sea}$) was calculated using the wind speed gas transfer velocity formula of Wanninkhof (2014):

$$\boldsymbol{F_{air-sea} = 0.251 U_{10}^2 \left(\frac{Sc}{660}\right)^{-0.5} K_0 (pCO_{2w} - pCO_{2a})} \quad (3)$$

with the squared wind speed at ten meter (U_{10}), the Schmidt number (Sc) polynomial of Wanninkhof (2014), the solubility coefficient of CO_2 (K_0) of Weiss (1974), the pCO_2 in air (pCO_{2a}) and the surface water pCO_2 (pCO_{2w}). The air-sea CO_2 flux and the correspondent change in DIC could only be calculated for the melt season of 2017 when wind speed data were available from Tempelfjorden. Measured wind speed at 10 m was obtained from a weather station at the opening of the fjord (https://www.unis.no/resources/weather-stations). The mean squared wind speed for the period of 43 $m^2\ s^{-2}$ was used in the calculations and a mean atmospheric pCO_2 of 399 µatm was also used. The latter value was approximated using the weather data in Tempelfjorden (i.e. vapour pressure was calculated from relative humidity, air pressure, and temperature at 5 m according to WMO-No. 8, 2014) and xCO_2 for dry air was obtained from the Zeppelin Observatory, Spitsbergen (NILU – Norwegian Institute for Air Research, http://ebas.nilu.no/). The calculated fluxes over the melt season ranged between -11 and -17 mmol m^{-2} day^{-1} with an average of -15.5±1.3 mmol m^{-2} day^{-1}. The effect of ice on the air-sea CO_2 flux can be important, as shown by e.g. Butterworth and Miller (2016), but during this period only glacier ice was scattered over the fjord (Fig. 2a), at low concentrations, and its effect on the flux was therefore treated as negligible.

The correspondent rate of change in DIC ($\partial DIC_{air\text{-}sea}/\partial t$) due to CO_2 uptake was calculated from:

$$\boldsymbol{\frac{\partial DIC_{air-sea}}{\partial t} = \frac{F_{air-sea}}{\rho h_{BD}}} \quad (4)$$

where ρ is the seawater density and h_{BD} is the equivalent to the mixed layer depth after Randelhoff et al. (2017), which here is used as the upper bound of the depth to which absorbed CO_2 may reach. According to Randelhoff et al. (2017):

$$\boldsymbol{h_{BD} = \int_{Surface}^{60\,m} dz[\sigma_{\theta d} - \sigma_\theta(z)] / \Delta\sigma_\theta} \quad (5)$$

where the numerator is the buoyancy deficit, σ_θ is ρ – 1000 kg m^{-3}, $\sigma_{\theta d}$ is a deep water reference density (mean σ_θ over 45 to 55 m), and $\Delta\sigma_\theta$ is the difference between the surface density (mean σ_θ over 1 to 3 m) and $\sigma_{\theta d}$. The mean h_{BD} for the deeper stations, 333 and 335, was 15.1 ±2.1 m, and this value was used in

Equation 4. The average change rate in DIC was 0.042±0.003 μmol kg^{-1} hr^{-1}. This change in DIC due to the air-sea CO_2 flux was then removed from the DIC data in the upper 15 m (referred to as DIC^{-gasex}), using the above value and the first sampling occasion in June each year as a zero reference, i.e. only CO_2 uptake after this sampling occasion is considered. As will be seen later, this is needed to determine the end-member DIC value of the local freshwater source and to resolve the change in pCO_2 due to the freshwater addition. A correspondent Ω_{Ar} (Ω_{Ar}^{-gasex}) was also calculated, based on TA and DIC^{-gasex}. These properties were then also regressed against f_{fw}.

Any uncertainty in $\partial DIC_{air\text{-}sea}/\partial t$ would result from uncertainties in the calculated fluxes and the use of h_{BD} as an estimate of the depth to which absorbed CO_2 may be mixed down to. Assuming that these uncertainties are comparable to the situation in Adventfjorden, they would be around ±30% and ±6 m (±40%) for the flux and h_{BD}, respectively (Ericson et al., 2018). The resultant uncertainty in $\partial DIC_{air\text{-}sea}/\partial t$ would be ±50% or ±0.021 μmol kg^{-1} hr^{-1}.

3. Times series of the marine CO_2 system – the seasonal cycle

The time series of the measured (temperature, salinity, pH, TA, $\delta^{18}O$, $[NO_3^-]$, and $[Si(OH)_4]$) and calculated (freshwater fraction, DIC, Ω_{Ar}, pCO_2, and Revelle factor) parameters are presented in Figures 3-5 for Stations 336, 333, and 335, respectively. The Stations 332 and 334 were not sampled frequently enough to produce a time series with seasonal resolution (see Table 1 for details) and data from these

stations are therefore not shown but used in Section 4. White areas in the Figures 3-5 are periods without data, for instance no sampling took place over the first half year of 2017.

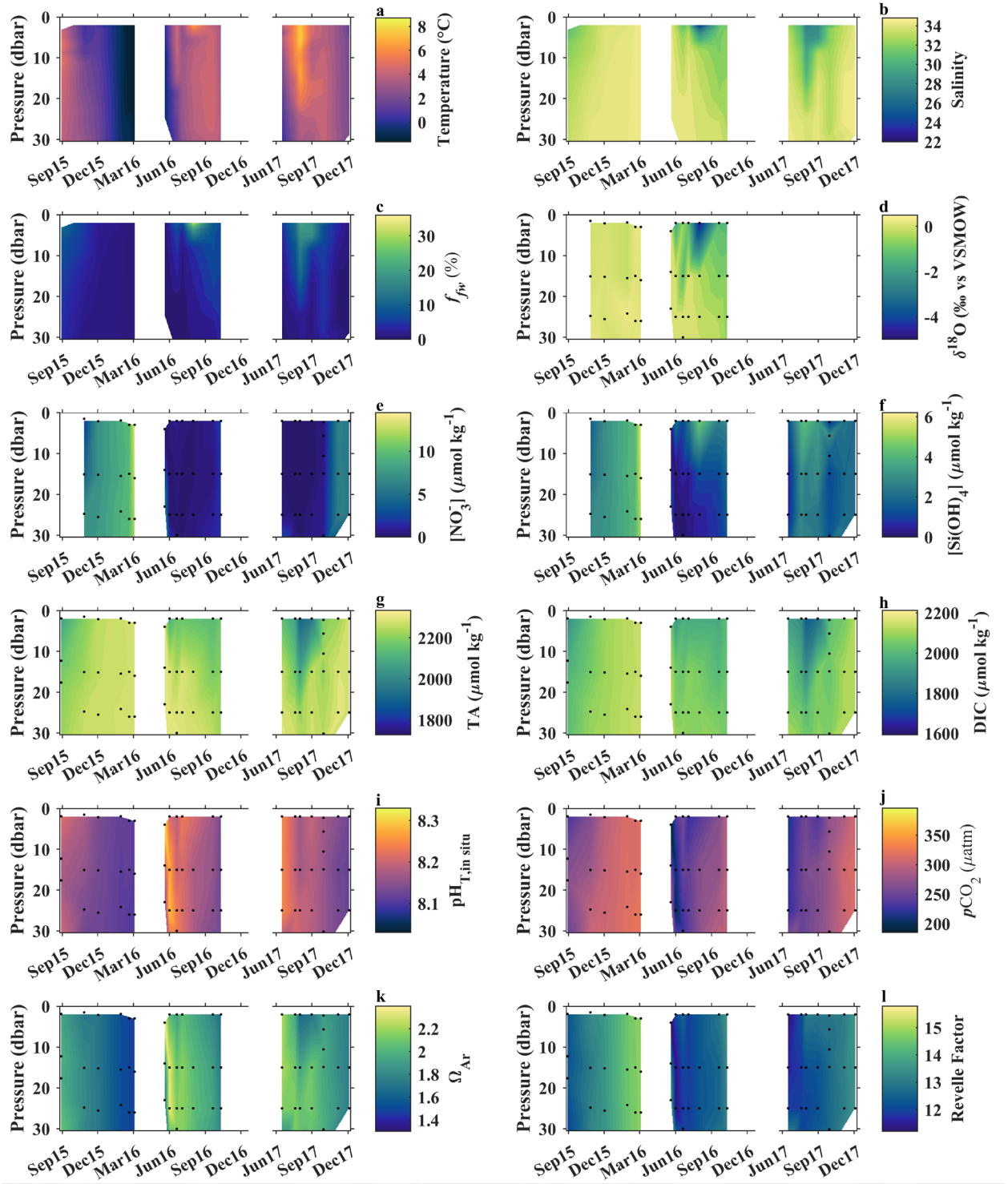

Fig. 3. Water column properties (2-30 m) at Station 336 between 29 August 2015 and 5 December 2017 including a) temperature, b) salinity, c) f_{fw} (freshwater fraction), d) $\delta^{18}O$, e) $[NO_3^-]$, f) $[Si(OH)_4]$, g) TA, h) DIC, i) pH, j) pCO_2,

k) Ω_{Ar}, and l) the Revelle Factor. Black dots show the timing of sampling as well as the sampling depths. No temperature measurements exist for 7 November 2017.

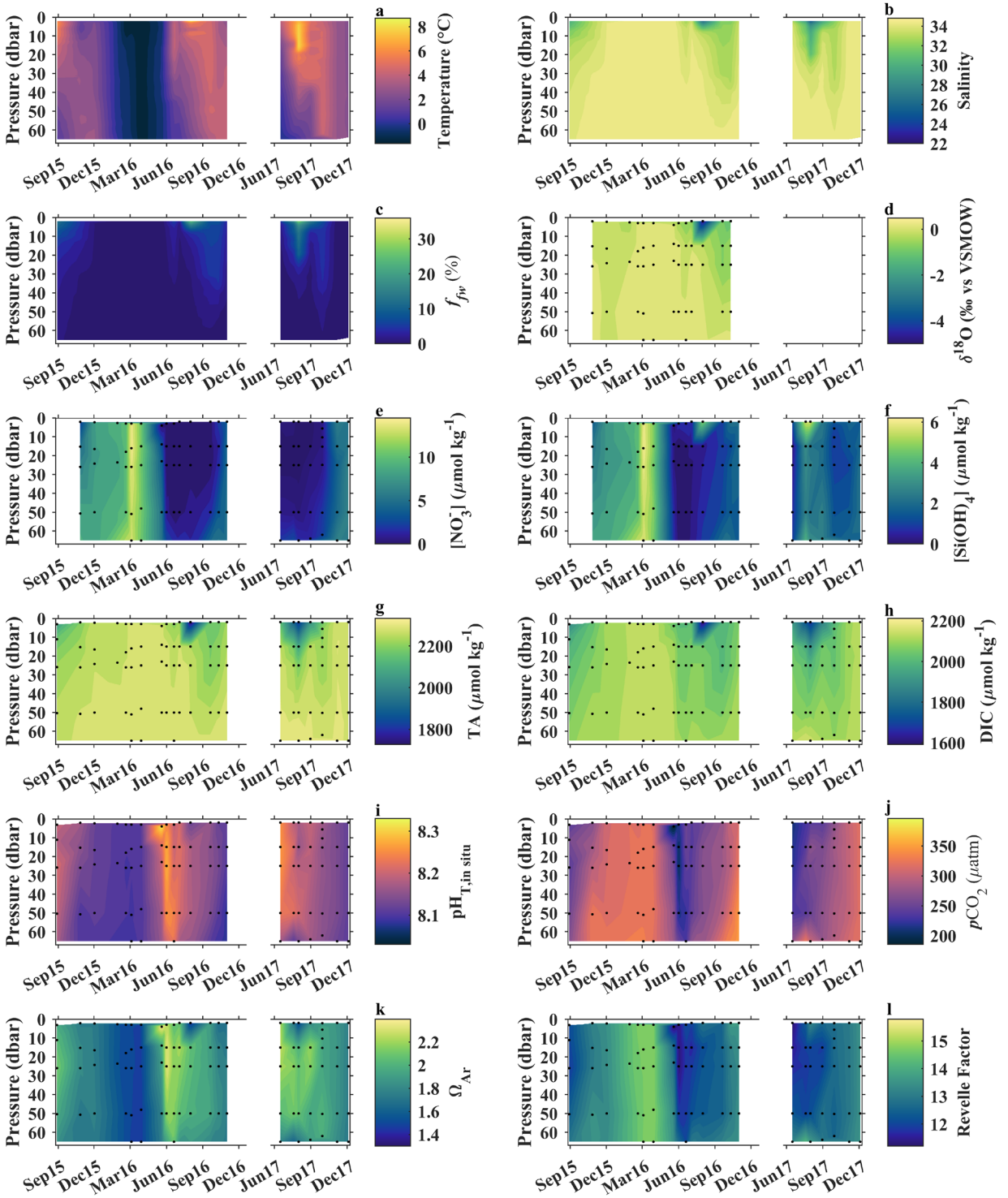

Fig. 4. Water column properties (2-60 m) at Station 333 between 29 August 2015 and 5 December 2017 including a) temperature, b) salinity, c) f_{fw} (freshwater fraction), d) $\delta^{18}O$, e) $[NO_3^-]$, f) $[Si(OH)_4]$, g) TA, h) DIC, i) pH, j) pCO_2,

k) Ω_{Ar}, and l) the Revelle Factor. Black dots show the timing of sampling as well as the sampling depths. No temperature measurements exist for 7 November 2017.

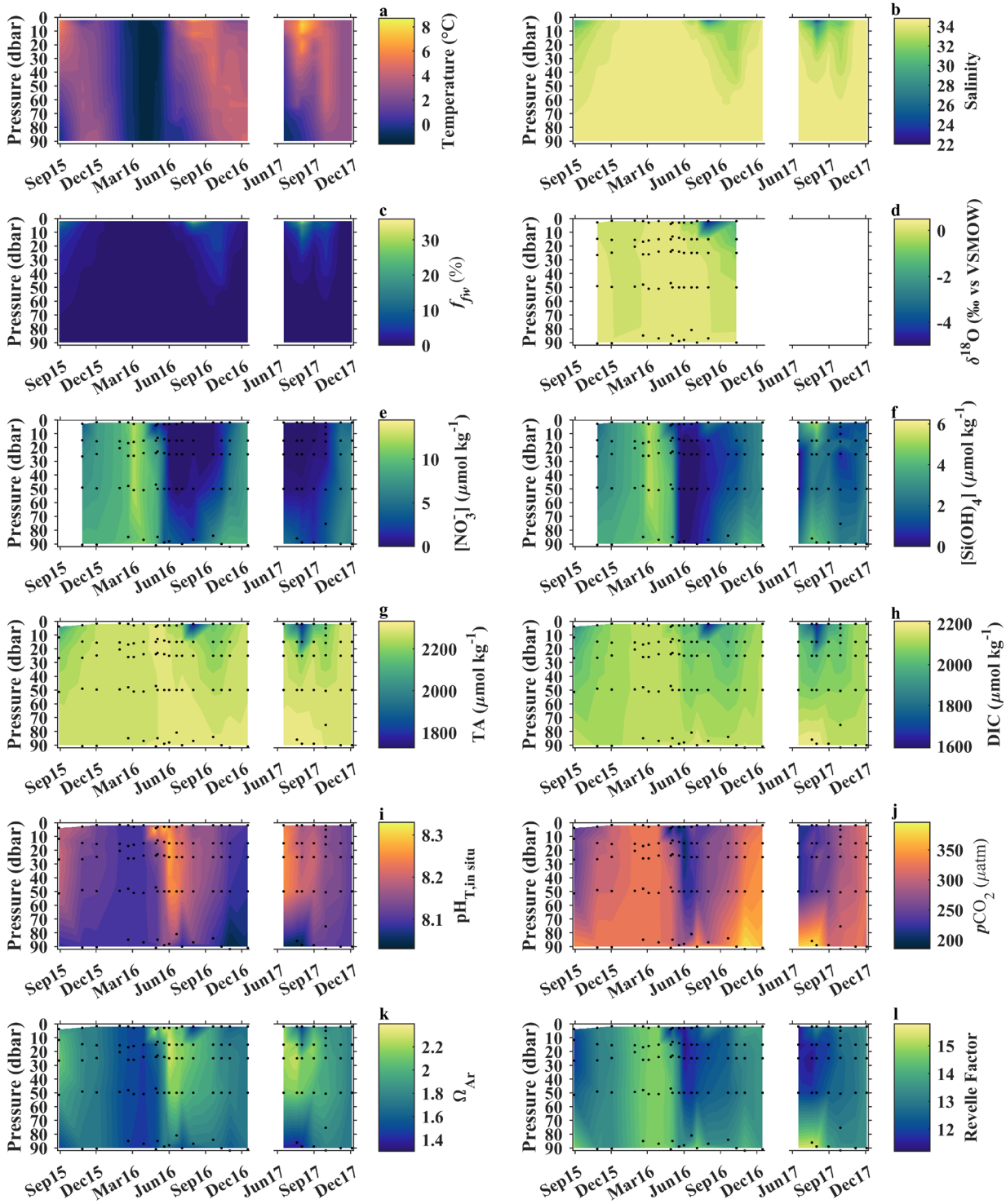

Fig. 5. Water column properties (2-90 m) at Station 335 between 29 August 2015 and 5 December 2017 including a) temperature, b) salinity, c) f_{fw} (freshwater fraction), d) $\delta^{18}O$, e) $[NO_3^-]$, f) $[Si(OH)_4]$, g) TA, h) DIC, i) pH, j) pCO_2, k) Ω_{Ar}, and l) the Revelle Factor. Black dots show the timing of sampling as well as the sampling depths. No temperature measurements exist for 7 November 2017.

3.1 Winter water mass properties from December to March: 2015/2016

Over the winter months a gradual cooling took place with temperatures from above 1°C in December to values between -0.2°C and -1.6 in February. The lowest temperature was observed at the surface at the innermost Station 336, near the glacier front. The cooling continued until Station 336 was covered by fast sea ice by the end of March. At this time, the mid-Station 333 and outermost Station 335 had temperatures between -1.5 and -1.3°C, with the former being slightly colder. Salinity and $\delta^{18}O$ ranged from about 34.0-34.6 and 0.0-0.2‰ in December, with lower values at the surface and close to the fjord head. The water column was more homogenous by the end of March, with salinity around 34.6 and $\delta^{18}O$ values of 0.2-0.3‰. Note that low $\delta^{18}O$ values of -0.1‰ were observed in January especially in the surface at all stations, which likely reflect glacial melt contributions, and also in the deeper water of Stations 336 (i.e. at 39 m) and 335 (i.e. at 50 m).

The $[NO_3^-]$ increased over the winter months from about 7.5-9.5 µmol kg^{-1} in December to 10.5-11.3 µmol kg^{-1} in the end of March 2016 (Figs. 3e, 4e, 5e). The corresponding $[Si(OH)_4]$ increased from 3.0-3.9 µmol kg^{-1} in December to 4.7-5.0 µmol kg^{-1} in the end of March. Fjord water TA (Figs. 3g, 4g, 5g) and DIC (Figs. 3h, 4h, 5h) were 2260-2290 µmol kg^{-1} and 2100-2150 µmol kg^{-1}, respectively, with values in the lower range in December especially at the innermost station and in the surface. By the end of March, the water column at the ice-free part of the fjord had become uniform with regard to TA and DIC that were in average 2291 ±1 and 2157±1 µmol kg^{-1}, respectively.

3.2 Spring water mass properties from April to May: 2016

Between the end of March and the end of April at the outermost Station 335, which was not covered by sea ice, the salinity had increased by 0.1 to a value of 34.7 and the temperature had increased by 0.3-0.5°C to values from -1.0 to -0.8°C. The nutrient concentrations in the surface for $[NO_3^-]$ and $[Si(OH)_4]$ had decreased from about 11.0 to 0.5 and 4.9 to 1.3 µmol kg^{-1}, respectively, which show that a phytoplankton bloom had already used up most of the nutrients. The low nutrient concentrations coincided with a high density of phytoplankton (visual observation). The change in $[NO_3^-]$ due to biological NO_3^- assimilation was similar in magnitude but in opposite direction to the change in surface water TA, which had increased by 12 µmol kg^{-1} to a value of 2303 µmol kg^{-1} (i.e. TA increases by 1 mole per 1 mole assimilated NO_3^- during primary production). Surface water DIC on the other hand, had

decreased by 85 µmol kg^{-1} to a value of 2073 µmol kg^{-1} due to biological CO_2 fixation. The calculated C:N ratio, i.e. $\Delta DIC:\Delta[NO_3^-]$ between the end of March and the end of April, was 8.1 assuming that the effect of air-sea CO_2 exchange on DIC was insignificant in comparison to the change in DIC due to primary production. This is a reasonable assumption considering the homogenous state of the water column, in terms of temperature, salinity, and TA, at the time, which suggests that any oceanic CO_2 uptake would be distributed over the entire water column. The effect of these changes in surface water TA and especially DIC, resulted in a reduction in surface water pCO_2 and the Revelle factor from about 330 µatm and 14.8, respectively, in late March, to 187 µatm and 11.4, respectively, in late April. The correspondent *in situ* pH and Ω_{Ar} had increased from 8.11 to 8.32 and 1.50 to 2.35, respectively.

A couple of weeks later most of the sea ice in the fjord was gone and the temperature ranged between -0.7 and 0.1°C. The correspondent salinity was generally > 34.7 except for the surface water where the salinity was close to 34.6. At this time $\delta^{18}O$ in the surface was between 0.1 and 0.2‰., whereas the rest of the fjord waters had values larger than 0.2‰ (Figs. 3d, 4d, and 5d). The impact of the phytoplankton bloom in terms of low nutrient concentrations was evident in the surface all the way to the innermost station. DIC was around 2070 µmol kg^{-1} in the surface, which concurred with maxima in pH and Ω_{Ar} of 8.32 and 2.41, respectively, and minima in pCO_2 and the Revelle Factor of 186 µatm and 11.3 respectively.

3. 3 Summer water mass properties from June to August: 2016 and 2017

In summer the gradual warming and freshening of the upper water column resulted in a pronounced stratification and the observed maxima in temperature and minima in salinity occurred in the surface in the beginning of August, regardless of year. The temperature reached maxima varying between 6.8 and 8.7°C, with values in the lower range at the innermost station. The freshest water was also observed at this station, with a maximum freshwater fraction of 36% (Fig. 3c) and a minimum salinity of 22.1 in 2016, which coincided with $\delta^{18}O$ of -4.6‰ (Fig. 3d). The minimum in $\delta^{18}O$ of -4.9‰ was also observed at this time in the surface at the outermost Station 335, which concurred with a salinity of 24.5. This was also the station where the freshest water was observed in 2017 (minimum in salinity and freshwater fraction of 23.9 and 31%), despite its location at the opening of the fjord.

In mid-June fjord water DIC was less than 2100 µmol kg^{-1} and $[NO_3^-]$ was < 1 µmol kg^{-1}, except for the bottom waters. $[Si(OH)_4]$ was also low at this time, i.e < 1 µmol kg^{-1}, although higher values were not only observed in the bottom waters, but also in the surface. In terms of the $[NO_3^-]$, the early summer state was sustained throughout the melt season. The supply of dissolved silica from the dominant freshwater source on the other hand resulted in surface $[Si(OH)_4]$ of up to 5.8 µmol kg^{-1}. DIC was

considerably diluted by the freshwater addition, reaching surface water minima in the beginning of August of 1593 µmol kg^{-1} in 2016 and 1633 µmol kg^{-1} in 2017. These minima concurred with minima in TA of ~1728 µmol kg^{-1} in 2016 and 1767 µmol kg^{-1} in 2017. The corresponding surface water pCO_2, pH, Ω_{Ar}, and the Revelle Factor for 2016 were 257 µatm, 8.13, 1.45, and 12.9, respectively. In 2017, the DIC minimum concurred with surface water pCO_2, pH, Ω_{Ar}, and the Revelle Factor of 240 µatm, 8.17, 1.48, and 13.4, respectively. Altogether, this shows that the surface pCO_2 and Revelle Factor had increased since the end of spring, whereas both pH and Ω_{Ar} had decreased over the same period.

One striking feature in the deep water in the summer season was very high TA and DIC values of 2324 µmol kg^{-1} and 2187 µmol kg^{-1}, respectively in 2016, and 2333 µmol kg^{-1} and 2213 µmol kg^{-1}, respectively in 2017. The especially high values in 2017 concurred with minima in *in situ* pH (Figs. 3i, 4i, 5i) and Ω_{Ar} (Figs. 3k, 4k, 5k) of 8.03 and 1.33, respectively, and maxima in pCO_2 (Figs. 3j, 4j, 5j) and the Revelle Factor (Figs. 3l, 4l, 5l) of 395 µatm and 15.1, respectively. This water had rather low temperatures down to -0.6°C and salinities about 34.8, which is a signature for water produced by cooling and freezing in winter.

3. 4 Autumn water mass properties from September to November: 2015, 2016, and 2017

Between autumn and early winter, the water column cooled down and there was a slow but steady increase in salinity as mixing due to wind stress, convection and/or advection worked to remove the stratified condition of the summer season. The nutrients, TA, DIC, pCO_2, and the Revelle Factor typically increased as the water column became more vertically homogenous, whereas *in situ* pH and Ω_{Ar} decreased.

4. Discussion

The importance of glacial meltwater effects on the marine CO_2 system has been acknowledged by several contributions including high air-sea CO_2 uptake (e.g. Rysgaard et al., 2012; Meire et al., 2015) as well as low Ω_{Ar} in waters with a high glacial meltwater content (e.g. Robbins et al., 2013; Evans et al., 2014; Fransson et al., 2015; Turk et al., 2016). The high CO_2 uptake is a result of low surface pCO_2, which to some extent is an effect of the high CO_2 solubility in less saline waters. For instance, Meire et al. (2015) observed for the Godthåbsfjord in Greenland a minimum in pCO_2 of less than 100 µatm that coincided with a salinity of less than 10. In Tempelfjorden such low salinities were not observed (minimum in salinity of 22, Fig. 3b). The annual minimum in pCO_2 (187 µatm, Fig. 5j), which concurred with a maximum in Ω_A (2.41, Fig. 5k), was observed in conjunction with the phytoplankton bloom (Fig. 5e), i.e. before the onset of the melt season. Primary production was therefore responsible for the largest changes observed in pCO_2 (a decrease of more than 140 µatm) and Ω_{Ar} (an increase of 0.9), which is in

line with observations from the neighbouring fjord branch, Adventfjorden (Fig. 1) (Ericson et al., 2018; Ericson et al., submitted to Polar Research).

The melt season in Tempelfjorden started when the CO_2 uptake capacity in terms of the air-sea pCO_2 gradient was at its maximum. In 2017, the "observed" surface pCO_2 increased by an average of 30 µatm between mid-June and the beginning of August. This increase in pCO_2 coincided with an increased temperature (mean value of 3.0°C) that would result in an increase in pCO_2 of about 28 µatm when using the relation from Takahashi et al. (1993; $d\ln pCO_2 / dT \approx 0.0423°C^{-1}$). Salinity, on the other hand, decreased by an average of 7.6 over the same period. To resolve the correspondent change in pCO_2 due to the freshwater addition, the end-member TA and DIC values of the freshwater are needed. To determine these values and to assess the dependence of TA, DIC, and Ω_{Ar} on the freshwater fraction, robust regressions (Table 2) were used on the data from June to the beginning of August (for the depths 2 - 30 m). To highlight the consequences of excluding the effect of air-sea CO_2 exchange on DIC and Ω_{Ar}, regressions with and without air-sea CO_2 exchange removed DIC and Ω_{Ar} are presented (Figure 6).

Table 2

Robust regression results for the upper water column (2 to 30 m) from June until 1st of August when salinity reached its yearly minimum: TA (µmol kg^{-1}) vs f_{fw}, DIC (µmol kg^{-1}) vs f_{fw}, and Ω_{Ar} vs f_{fw} for 2016 and 2017.

Year		Slope ±SE	*p*-value	Intercept ±SE	*p*-value	R^2	n
2016	TA vs f_{fw}	-1957 ±24	$2 \cdot 10^{-40}$	2312 ±2	$2 \cdot 10^{-81}$	0.99	36
2016	DIC vs f_{fw}	-1587 ±52	$2 \cdot 10^{-26}$	2095 ±4	$9 \cdot 10^{-69}$	0.97	36
2016	DIC^{-gasex} vs f_{fw}	-1769 ±73	$5 \cdot 10^{-23}$	2086 ±5	$1 \cdot 10^{-63}$	0.95	36
2016	$\Omega_{Ar,T=4°C}$ versus f_{fw}	-3.22 ±0.30	$2 \cdot 10^{-12}$	2.27 ±0.02	$6 \cdot 10^{-44}$	0.77	36
2016	$\Omega^{-gasex}_{Ar,T=4°C}$ versus f_{fw}	-1.58 ±0.44	0.001	2.36 ±0.03	$8 \cdot 10^{-39}$	0.27	36
2017	TA vs f_{fw}	-1702 ±41	$2 \cdot 10^{-24}$	2303 ±5	$1 \cdot 10^{-50}$	0.99	27
2017	DIC vs f_{fw}	-1422 ±45	$1 \cdot 10^{-21}$	2083 ±6	$2 \cdot 10^{-48}$	0.98	27
2017	DIC^{-gasex} vs f_{fw}	-1602 ±65	$5 \cdot 10^{-19}$	2077 ±8	$2 \cdot 10^{-44}$	0.96	27
2017	$\Omega_{Ar,T=4°C}$ versus f_{fw}	-2.79 ±0.14	$1 \cdot 10^{-16}$	2.30 ±0.02	$5 \cdot 10^{-37}$	0.94	27
2017	$\Omega^{-gasex}_{Ar,T=4°C}$ versus f_{fw}	-1.09 ±0.28	$8 \cdot 10^{-4}$	2.30 ±0.03	$1 \cdot 10^{-29}$	0.37	27

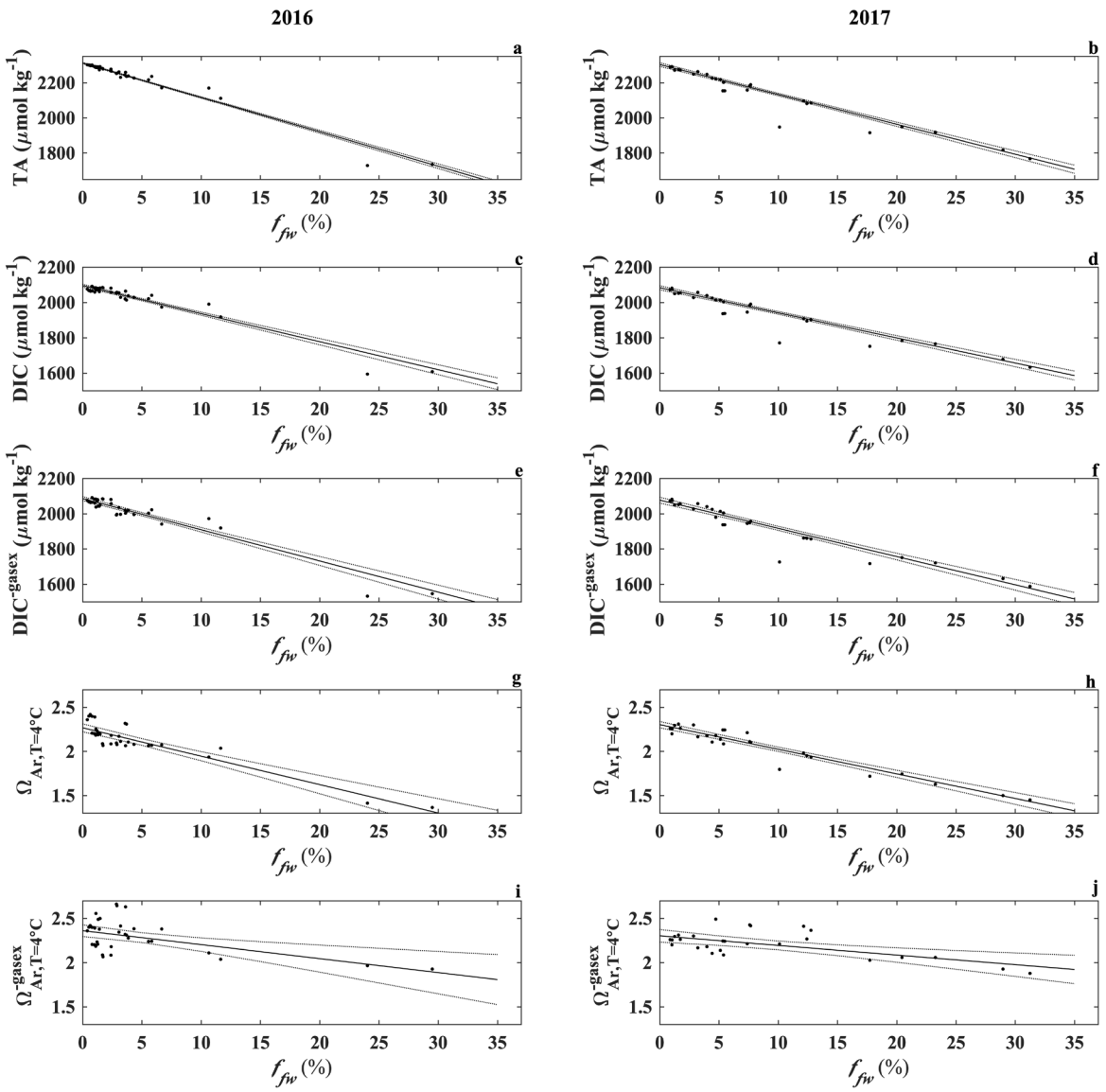

Fig. 6. Plots of melt season upper water column (depths from 2 to 30 m) properties: a) TA versus f_{fw} in 2016, b) TA versus f_{fw} in 2017, c) DIC versus f_{fw} in 2016, d) DIC versus f_{fw} in 2017, e) DIC^{-gasex} vs f_{fw} in 2016, f) DIC^{-gasex} vs f_{fw} in 2017, g) $\Omega_{Ar,T=4°C}$ versus f_{fw} in 2016, h) $\Omega_{Ar,T=4°C}$ versus f_{fw} in 2017, i) $\Omega^{-gasex}_{Ar,T=4°C}$ versus f_{fw} in 2016, and j) $\Omega^{-gasex}_{Ar,T=4°C}$ versus f_{fw} in 2017. Solid lines show robust regression results in Table 2, whereas the dotted lines show the 95% confidence intervals of the predicted regression lines.

The regressions showed that the freshwater in Tempelfjorden had a diluting impact on TA. Based on the relationships, the end-members for 2016 and 2017 were estimated to 355±24 and 601 ±42 µmol kg^{-1}, respectively (Fig. 6a, b, Table 2). These values agree fairly well with estimated end-members for Tempelfjorden in September 2013 (526 µmol kg^{-1}) by Fransson et al. (2015), and for Adventfjorden between 2015 and 2017 (418 µmol kg^{-1}) by Ericson et al. (submitted to Polar Research). The higher

freshwater contribution in 2017 could reflect the increased activity of Tunabreen (Fig.2f) that contains sediments enriched in calcite and ankerite/dolomite (Forwick et al., 2010). Similar to TA, DIC decreased with increasing freshwater content and the end-members were estimated to 508±52 and 661±45 µmol kg^{-1}, for 2016 and 2017, respectively (Fig. 6c, d, Table 2). When the effect of air-sea CO_2 uptake was removed from the DIC data, i.e. using DIC^{-gasex} in the regressions, these values decreased to 316 ±73 µmol kg^{-1} and 474±66 µmol kg^{-1}, for 2016 and 2017, respectively (Fig. 6e, f, Table 2). For a ±50% uncertainty in $\partial DIC_{air\text{-}sea}/\partial t$ (as mentioned in Section 2), the DIC^{-gasex} end-members would range between 238±96 and 405±55 µmol kg^{-1} and 371±76 and 574±52 µmol kg^{-1} for 2016 and 2017, respectively.

Using the TA and DIC^{-gasex} end-members above, the decrease in pCO_2 due to dilution over the melt season in 2017 was calculated to be around 77 µatm (for the ±50% uncertainty in $\partial DIC_{air\text{-}sea}/\partial t$ the decrease would be between 53 and 98 µatm). Combining the effects of temperature and dilution on the pCO_2 with the observed change in pCO_2 there must be a process or processes that increased pCO_2 by approximately 79 µatm. This increase in pCO_2 corresponds to an increase in DIC of 50 µmol kg^{-1} as estimated from the mean values of the surface properties (i.e. surface pCO_2, Revelle factor, and DIC of 231 µatm, 12.3 and 1816 µmol kg^{-1}, respectively). Based on the change rate in DIC of 0.042 µmol kg^{-1} hr^{-1} due to air-sea CO_2 uptake (using Eqs. 3-5) the DIC would increase by 47 µmol kg^{-1}. This number agrees well with the estimated increase in DIC of 50 µmol kg^{-1}. Assuming that the biological activity has minimal effects on the surface pCO_2 over the melt season, which is supported by the low $[NO_3^-]$ (< 1 µmol kg^{-1} in the upper 30 m) (Fig. 3e, 4e, 5e), as well as by estimates done for Adventfjorden (Ericson et al., 2018), and assuming that the effects of mixing on the surface pCO_2 are comparable to the situation in Adventfjorden (Ericson et al., 2018), and therefore insignificant, it is reasonable to conclude that air-sea CO_2 uptake and freshwater discharge were the key drivers of the surface pCO_2 at this time.

To estimate the impact of freshening over this period on the CO_2 uptake, surface pCO_2 was calculated using CO2SYS. The mean surface salinity in mid-June 2017 was used as input together with averaged TA and DIC, for which the effects of dilution first had been removed using the changes in salinity and the end-members above (i.e. for DIC the end-member of 474 µmol kg^{-1}). With this new surface pCO_2 the CO_2 uptake would decrease from about 47 to 35 µmol kg^{-1} (for the DIC end-members of 371 and 574 µmol kg^{-1} this value would range between 32 and 38 µmol kg^{-1}), which means that the freshening accounts for close to one fourth of the CO_2 uptake.

Changes in the Ω_{Ar}, through its proportional relation to the $[CO_3^{2-}]$, can largely be explained by changes in DIC and TA that often govern both the pH and the concentrations of the carbonate species (Zeebe and Wolf-Gladrow, 2001). Ω_{Ar} is, however, also affected by temperature. To remove this temperature effect the mean temperature in the upper water column over the melt season (T = 4.0°C) was

used, together with TA, DIC, and a pressure of 0 dbar, as input in CO2SYS to calculate Ω_{Ar} at 4.0°C ($\Omega_{Ar,T=4°C}$). The relationships between this calculated $\Omega_{Ar,T=4°C}$ and the freshwater fraction (Fig. 6g, h, Table 2) were negative with slopes of -0.032±0.003/%f_{fw} and -0.028±0.001/%f_{fw}, for 2016 and 2017, respectively. These values agree fairly well with the regression-based relation between Ω_{Ar} and the meteoric freshwater fraction (f_{mw}) of -0.032/% f_{mw} that Turk et al. (2016) found for Cumberland Sound. On the other hand, the values are higher than -0.009/% f_{fw} for Adventfjorden, as estimated by Ericson et al. (submitted to Polar Research) using conservative mixing between land runoff and seawater. The latter value is more consistent with the slope of -0.014/%f_{SIM} found by Chierici et al. (2011) for the Amundsen Gulf who used the linear relationship between solely salinity dependent changes in Ω_{Ar} and monthly changes in sea ice meltwater fraction (f_{SIM}).

The difference between these estimates could be that air-sea CO_2 uptake affects the regression based methods. In Adventfjorden, Ericson et al. (submitted to Polar Research) estimated that air-sea CO_2 uptake gave a monthly average decrease in Ω_{Ar} of 0.03±0.01 for the water column (i.e. 2 to 75 m) there. As the water column is stratified in the summer the change in the upper part is likely much larger than the average. In Tempelfjorden the relationships between $\Omega_{Ar,T=4°C}$ with the effect of the air-sea CO_2 flux removed ($\Omega^{-gasex}_{Ar,T=4°C}$) and f_{fw} resulted in negative slopes of -0.016±0.004/%f_{fw} and -0.011±0.003/%f_{fw} for 2016 and 2017, respectively (Fig. 6i, j, Table 2). Again, using the ±50% uncertainty in $\partial DIC_{air\text{-}sea}/\partial t$, the ranges would be from -0.025±0.003/%f_{fw} to -0.007±0.006/%f_{fw} and from -0.020±0.002/%f_{fw} to -0.002±0.004/%f_{fw} in 2016 and 2017, respectively.

When Ω_{Ar} gets below 1, the water will become undersaturated in aragonite and the mineral may dissolve. If air-sea CO_2 exchange is not accounted for the freshwater fraction that is needed in Tempelfjorden for the water to become aragonite undersaturated range between 39 ±4% and 47±2% in 2016 and 2017, respectively. These values are close to the correspondent regression-based estimate of the freshwater fraction for estuarine surface waters in Cumberland Sound of 37% (Turk et al., 2016), as well as to the air-sea exchange independent estimate for the sea ice meltwater fraction of 40% as estimated from conservative mixing by Azetsu-Scott et al. (2010). However, the relationships for Tempelfjorden with air-sea CO_2 exchange removed, show that much higher freshwater fractions are needed to reach undersaturation. In 2016 the freshwater fraction needed was estimated to 86±24% and in 2017 a 100% freshwater was not enough to produce aragonite undersaturated waters. For the ±50% uncertainty in $\partial DIC_{air\text{-}sea}/\partial t$ the lower ranges of these fractions would be 54±6 % and 66±7% for 2016 and 2017, respectively, whereas the upper ranges would exceed 100%.

Even though it is common to use correlation or regression techniques to show the relationship between different types of meltwater (sea ice melt water or meteoric water) on the ocean acidification

state/carbonate chemistry (e.g. Fig. 1B in Yamamoto-Kawai et al. 2009; Table 4 in Robbins et al., 2013; Fig 6 and Table 3 in Turk et al., 2016), the examples above show that the interpretation of such relationships will be sensitive to the effect of air-sea exchange. Especially since the freshwater: 1) contributes with a higher CO_2 solubility, 2) is often mixed with seawater with low pCO_2 as a result of previous primary production (e.g. Shadwick et al., 2011; Meire et al. 2015; Ericson et al., 2018), and 3) resides in the surface where it is in contact with the atmosphere for the longest period and subsequently more exposed to air-sea CO_2 exchange.

During the summer season, especially in 2017, high values of TA and DIC can be seen in the deepest water of the outer basin especially at Station 335 (Fig. 5 g, h, i, k) coinciding with minima in pH and Ω_{Ar}. The stations where these high TA and DIC were found are shown in Table 3. The TA and DIC varied between 2324 - 2333 µmol kg^{-1} and 2185 - 2213 µmol kg^{-1}, respectively. These high concentrations occurred in rather saline waters (S≥34.7) with temperatures from -0.6 to 0.3°C.

Table 3

Properties of bottom water at stations (Stn) with high TA (µmol kg^{-1}) and DIC (µmol kg^{-1}), including pressure (P, dbar), temperature (T, °C), salinity (S), [NO_3^-] (µmol kg^{-1}) and salinity normalized and nutrient corrected TA and DIC. The correspondent average values for winter water (December to March) is also presented.

Date	Stn	P	T	S	[NO_3^-]	TA	DIC	$TA^{norm,corr}$	$DIC^{norm,corr}$
4 Jul 2016	335	90	0.2	34.7	3.4	2324	2187	2323	2235
16 Jun 2017	335	94	-0.6	34.8	5.7	2328	2213	2322	2239
20 Jul 2017	333	68	0.3	34.7	3.1	2325	2185	2328	2239
20 Jul 2017	335	86	0.0	34.7	3.8	2330	2202	2329	2248
1 Aug 2017	335	89	0.2	34.7	3.0	2333	2209	2333	2261
Winter water	All			34.5±0.1	9.8±2.3	2284±7	2138±16	2306±4	2158±10

Excessively high DIC content in the deep water of Arctic fjords was first acknowledged by Anderson et al. (2004) for Storfjorden, on the east coast of Spitsbergen. They observed a 10 µmol kg^{-1} increase in the salinity normalized and nutrient corrected deep water DIC in April 2002. This was attributed to an enhanced air-sea CO_2 uptake in the cold surface film that surrounds ice crystals at formation in combination with the export of brine-enriched high salinity waters to the deep. Omar et al. (2005) assessed an increase of 17 µmol kg^{-1} for the same fjord due to uptake of CO_2 through sea ice

production. Also, Rysgaard et al. (2007) found evidence for the production of DIC-enriched brine and the subsequent rejection thereof from growing sea ice, which may sink to the bottom water.

To provide an understanding of the origin of the excess TA and DIC observed in Tempelfjorden, the TA and DIC values in Table 3 were salinity normalized (S_{ref} = 34.8) and nutrient corrected according to Eqs. 6 and 7:

$$\mathbf{TA^{norm,corr}} = \mathbf{(TA^{meas} + (NO_3^{meas} - NO_3^{ww})/34.8/S^{meas}} \quad (6)$$

$$\mathbf{DIC^{norm,corr}} = \mathbf{\left(DIC^{meas} - R_{C/N}(NO_3^{meas} - NO_3^{ww}\right)/34.8/S^{meas}} \quad (7)$$

where NO_3^{ww} refers to winter water (mean nitrate concentration averaged over the period December to March) and $R_{C/N}$ is the Redfield ratio of 6.625 (Redfield et al., 1963). This ratio agrees well with the estimated spring bloom C:N uptake ratio of TAW (6.6) at the neighbouring fjord branch, Adventfjorden in 2016 (Ericson et al., submitted to Polar Research).

The normalized and corrected DIC varied between 2235 and 2261 µmol kg^{-1}, whereas TA changed only slightly (< 7 µmol kg^{-1}, Table 3). As a reference, all winter TA and DIC data (December to March) were also salinity normalized and nutrient corrected (Eqs. 6, 7) with the mean values presented in Table 3. In winter, the normalized and corrected TA and DIC were on average 2306±4 µmol kg^{-1} and 2158±10 µmol kg^{-1}, respectively. That means that the normalized and nutrient corrected deep water TA and DIC in the summer on average were 22 µmol kg^{-1} and 86 µmol kg^{-1}, respectively, higher than the winter averages. These high values could result from sea ice release of brine enriched in TA and especially DIC as observed by for instance Miller et al. (2011). The excess in TA could also be a result of released carbonate ions (CO_3^{2-}) from either dissolution of ikaite crystals (a $CaCO_3$ mineral) that have been previously formed in the brine pockets of sea ice (e.g Dieckmann et al., 2010) or from eroded bedrock minerals provided by Tunabreen and von Postbreen (ankerite/dolomite and calcite, Forwick et al., 2010; Fransson et al., 2015). This is however a less likely scenario since the dissolution of the minerals is expected to take place in the less saline upper water column rather than in the deep water. Still, such an addition of CO_3^{2-} would explain about 11 µmol kg^{-1} of the excess in DIC (i.e. since a change in $[CO_3^{2-}]$ affects TA by a factor of 2 and DIC by a factor of only 1). The excess in DIC, i.e. between on average 75 and 86 µmol kg^{-1} depending on cause, could thus be a result of oceanic CO_2 uptake and/or addition through release of DIC-enriched sea ice brine. Unfortunately, data over the period of sea ice production in 2017 are missing and hence it is difficult to confirm that the excess in DIC do result from this season. It should however be noted that the sea ice cover, although variable for this year was more extensive compared to 2016. That is the fast sea ice in the end of March 2017 not only covered Tempelfjorden, but

also most parts of the connecting Sassenfjorden, which also shares the outer basin. The deep water of this basin is largely confined by a shallow sill at the outer part of Sassenfjorden.

To put the estimated excess of DIC into a context, Fransson et al. (2015) observed for Tempelfjorden in April 2013, maxima in TA and DIC of about 2332 and 2205 μmol kg^{-1}, respectively. This was a year when the sea ice cover also was extensive, and these maxima were found below the sea ice at 10 m. If these TA and DIC values were salinity normalized and nutrient corrected (Eqs. 6, 7), the resultant values would be 2325 and 2213 μmol kg^{-1}, respectively. The excess in TA from the April 2013 data in Fransson et al. (2015) is similar to that observed in the deep water in the summer in the present study, whereas the excess in DIC, would be about 55 μmol kg^{-1} or, if corrected for approximately 10 μmol kg^{-1} due to released CO_3^{2-}, about 45 μmol kg^{-1}. This is less than what was observed in the summer season over the present study (between 75 and 86 μmol kg^{-1}), but their measurements are from the upper part of the water column. The excess in TA and DIC found in April 2013 could result from sinking brine. The high DIC in the summer of 2017 on the other hand, could reflect an accumulation of dense water enriched in DIC in the deepest part of the fjord. This water likely has a DIC-signature both from the production of brine as well as through enhanced atmospheric CO_2 uptake during freezing.

5. Conclusions

This study highlights that without the knowledge of the DIC end-member, any assumptions on sensitivities of the marine CO_2 system on the different types of freshwater will likely be biased by the effect of air-sea CO_2 exchange. There is therefore a need of numerous measurements of river, glacier, and sea ice TA and especially DIC for the determination of representative end-members. A way around this problem is to estimate the air-sea CO_2 exchange, however, large uncertainties (20% or more, e.g. Wanninkhof, 2014) exist for flux estimates that are based on different wind-speed parameterisations of the gas transfer velocity. Also, without direct measurements of turbulence, it is difficult to accurately determine the depth to which absorbed gases may be mixed down, which not necessarily agrees with the existing options of mixed layer depth determinations that use CTD-data.

Still, this study shows that the air-sea CO_2 uptake (on average 15.5 mmol m^{-2} day^{-1} in 2017) in Tempelfjorden over the period of peak freshwater discharge (June to the beginning of August) was large and that the freshening in itself accounted for about 25% of the uptake. If the effect of air-sea CO_2 uptake was removed from Ω_{Ar} at least 50% (lower range of uncertainty) of freshwater was needed for the fjord water to become aragonite undersaturated. When the glacial activity of the tidewater-glacier Tunabreen increased as observed in 2017, the amount of freshwater increased to at least 60% (lower range of

uncertainty) and the freshwater likely provided enough carbonate minerals to maintain Ω_{Ar} above 1 regardless of the freshwater fraction.

The data also show deep water with an excess of on average 86 μmol kg^{-1} in the salinity normalized and nutrient corrected DIC. This water was found in the summer season close to the bottom mainly in 2017. Since this year had an extensive period of sea ice growth, the excess is attributed to DIC-enriched brine release together with an enhanced CO_2 uptake during freezing over the period of sea ice growth. This efficient CO_2 sink will likely disappear if the sea ice production continues to decrease as already observed for this part of the Arctic.

Acknowledgments

The fieldwork was financially supported by the Norwegian Research Council under Arctic Field Grant (RiS #: 10662), with additional help from course activities at the University Centre in Svalbard (UNIS), and the Ocean Acidification flagship within the FRAM- High North Centre for Climate and the Environment, Norway (A. Fransson, M. Chierici). Metadata are accessible at the RiS portal at www.researchinsvalbard.no, and all data will be available on the Norwegian Marine Data Centre (NMDC) within half a year after publication. Until then contact the corresponding author for access to the data. We gratefully thank the logistic department at UNIS for all support with the fieldwork. Finally, we gratefully acknowledge the valuable comments and suggestions from Wiley Evans and an anonymous reviewer.

References

Anderson, L.G., Falck, E., Jones, E.P., Jutterström, S., Swift, J.H., 2004. Enhanced uptake of atmospheric CO_2 during freezing of seawater: A filed study in Storfjorden, Svalbard. J. Geophys. Res. 109, C06004. doi:10.1029/2003JC002120

Arrigo, K.R., van Dijken, G.L., Castelao, R.M., Luo, H., Rennermalm, Å.K., Tedesco, M., Mote, T.L., Oliver, H., Yager, P., 2017. Melting glaciers stimulate large summer phytoplankton blooms in southwest Greenland waters. Geophys. Res. Lett. 44, 6278-6285. doi:10.1002/2017GL073583

Azetsu-Scott, K., Clarke, A., Falkner, K., Hamilton, J., Jones, E.P., Lee, C., Petrie, B., Prinsenberg, S., Starr, M., Yeats, P., 2010. Calcium carbonate saturation states in the waters of the Canadian Arctic Archipelago and the Labrador Sea. J. Geophys. Res. 115, C11021. doi:10.1029/2009JC005917

Bendschneider, K., Robinson, R.I., 1952. A new spectrophotometric method for determination of nitrite in seawater. J. Mar. Res. 2, 87-96.

Butterworth, B.J., Miller, S.D., 2016. Air-sea exchange of carbon dioxide in the Southern Ocean and Antarctic marginal ice zone. Geophys. Res. Lett. 43, 7223-7230. doi:10.1002/2016GL069581

Chen, B., Cai, W.-J., Chen, L., 2015. The marine carbonate system of the Arctic Ocean: Assessment of internal consistency and sampling considerations, summer 2010. Mar. Chem. 176, 174-188. http://dx.doi.org/10.1016/j.marchem.2015.09.007

Chierici, M., Fransson, A., Anderson, L.G., 1999. Influence of *m*-cresol purple indicator additions on the pH of seawater samples: correction factors evaluated from a chemical speciation model. Mar. Chem. 65, 281-290. https://doi.org/10.1016/S0304-4203(99)00020-1

Chierici, M., Fransson, A., Lansard, B., Miller, L.A., Mucci, A., Shadwick, E., Thomas, H., Tremblay, J.-E., Papakyriakou, T.N., 2011. Impact of biogeochemical processes and environmental factors on the calcium carbonate saturation state in the Circumpolar Flaw Lead in the Amundsen Gulf, Arctic Ocean. J. Geophys. Res. 116, C00G09. doi:10.1029/2011JC007184

Clayton, T.D., Byrne R.H., 1993. Spectrophotometric seawater pH measurements: Total hydrogen ion concentration scale calibration of *m*-cresol purple and at-sea results. Deep Sea Res. Part I 40(10), 2115–2129. https://doi.org/10.1016/0967-0637(93)90048-8

Cottier, F.R., Tverberg, V., Inall, M.E., Svendsen, H., Nilsen, F., Griffiths, C., 2005. Water mass modification in an Arctic fjord through cross shelf exchange: The seasonal hydrography of Kongsfjorden, Svalbard. J. Geophys. Res. 110, C12005. https://doi.org/10.1029/2004JC002757

Dickson, A.G., 1990. Standard potential of the reaction: AgCl(s) + 1/2H_2 (g) = Ag(s) + HCl(aq), and the standard acidity constant of the ion HSO_4^- in synthetic sea water from 273.15 to 318.15 K. J. Chem. Thermodynamics 22, 113–127. https://doi.org/10.1016/0021-9614(90)90074-Z

Dickson, A.G., Millero, F.J., 1987. A comparison of the equilibrium constants for the dissociation of carbonic acid in seawater media. Deep Sea Res. Part A 34(10), 1733–1743. https://doi.org/10.1016/0198-0149(87)90021-5

Dieckmann, G.S., Nehrke, G., Uhlig, C., Göttlicher, J., Gerland, S., Granskog, M.A., Thomas, D.N., 2010. Brief communication: ikaite ($CaCO_3 * 6H_2O$) discovered in Arctic sea ice. The Cryosphere 4, 227–230.

DOE (U.S. Department of Energy), 1994. Handbook of methods for the analysis of the various parameters of the carbon dioxide system in sea water, version 2. Dickson, A.G., Goyet, C. (Eds.), ORNL/CDIAC-74.

Doney, S.C., Balch, W.M., Fabry, V.J., Feely, R.A., 2009. Ocean acidification: A critical emerging problem for the ocean sciences. Oceanography 22(4), 16-25.

Ericson, Y., Chierici, M., Falck, E., Fransson, A., Jones, E., Kristiansen, S., 2018. Evolution of the marine CO_2 system in a West Spitsbergen fjord with emphasis on seasonal drivers of the calcium carbonate saturation state. Submitted to Polar Research.

Ericson, Y., Falck, E., Chierici, M., Fransson, A., Kristiansen, S., Platt, S.M., Hermansen, O., Myhre, C. L., 2018. Temporal variability in surface water pCO_2 in Adventfjorden (West Spitsbergen) with emphasis on physical and biogeochemical drivers. J. Geophys. Res. Oceans 123. https://doi.org/10.1029/2018JC014073

Evans, W., Mathis, J.T., Cross, J.N., 2014. Calcium carbonate corrosivity in an Alaskan inland sea. Biogeosciences 11, 365-379. doi:10.5194/bg-11-365-2014

Ewertowski, M., 2014. Recent transformations in the high-Arctic glacier landsystem, Ragnabreen, Svalbard. Geografiska Annaler: Series A, Physical Geography 96, 265-285. doi:10.1111/geoa.12049

Forwick, M., Vorren, T.O., Hald, M., Korsun, S., Roh, Y., Vogt, C., Yoo, K.-C., 2010. Spatial and temporal influence of glaciers and rivers on the sedimentary environment in Sassenfjorden and Tempelfjorden, Spitsbergen. In: Howe, J.A., Austin, W.E.N., Forwick, M., Paetzel, M., (Eds) Fjord Systems and Archives. Geological Society, London, Special Publications 344, 163–193. http://doi.org/10.1144/SP344.13

Fransson, A., Chierici, M., Hop, H., Findlay, H.S., Kristiansen, S., Wold, A., 2016. Late winter-to-summer change in ocean acidification state in Kongsfjorden, with implications for calcifying organisms. Polar Biol. 39(10), 1841-1857.

Fransson, A., Chierici, M., Nomura, D., Granskog, M.A., Kristiansen, S., Martma T., Nehrke, G., 2015. Effect of glacial drainage water on the CO_2 system and ocean acidification state in an Arctic tidewater-glacier fjord during two contrasting years. J. Geophys. Res. Oceans 120. https://doi.org/10.1002/2014JC010320

Grabiec, M., Ignatiuk, D., Jania, J.A., Moskalik, M., Glowacki, P., Blaszczyk, M., Budzik, T., Walczowski, W., 2017. Coast formation in an Arctic area due to glacier surge and retreat: The Hornbreen-Hambergbreen case from Spitsbergen, Earth Surf. Process. Landforms 43, 387-400. doi:10.1002/esp.4251

Grasshof, K., 1965. On the automatic determination of phosphate, silicate and fluoride in seawater. ICES Hydrographic Committee Report No. 129.

Grasshof, K., Kremling, K., Ehrhardt, M., 2009. Methods of Seawater Analysis, third ed. John Wiley, New York.

Lee, K., Kim, T.-W., Byrne, R.H., Millero, F.J., Feely, R.A., Liu, Y.-M., 2010. The universal ratio of boron to chlorinity for the North Pacific and North Atlantic oceans. Geochimica et Cosmochimica Acta 74, 1801-1811.

Lund-Hansen, L.C., Hawes, I., Holtegaard Nielsen, M., Dahllöf, I., Sorrell, B.K., 2018. Summer meltwater and spring sea ice primary production, light climate and nutrients in an Arctic estuary, Kangerlussuaq, west Greenland. Arctic, Antarctic, and Alpine Research 50(1), S100025. doi:10.1080/15230430.2017.1414468

Marlin, C., Tolle, F., Griselin, M., Bernard, E., Saintenoy, A., Quenet, M., Friedt, J.-M., 2017. Change in geometry of a high Arctic glacier from 1948 to 2013 (Austre Lovénbreen, Svalbard). Geografiska Annaler: Series A, Physical Geography 99(2), 115-138.

Mehrbach, C., Culberson, C.H., Hawley, J.E., Pytkowicz, R.M.. 1973. Measurement of the apparent dissociation constants of carbonic acid in seawater at atmospheric pressure. Limnol. Oceanogr. 18, 897–907. https://doi.org/10.4319/lo.1973.18.6.0897

Meire, L., Søgaard, D.H., Mortensen, J., Meysman, F.J.R., Soetaert, K., Arendt, K.E., et al., 2015. Glacial meltwater and primary production are drivers of strong CO_2 uptake in fjord and coastal waters adjacent to the Greenland Ice Sheet. Biogeosciences 12, 2347-2363. doi:10.5194/bg-12-2347-2015

Menard, H.W., Smith, S.M., 1966. Hypsometry of ocean basin provinces. J. Geophys. Res. 71(18), 4305-4325.

Miller, L.M., Carnat, G., Else, B.G.T., Sutherland, N., Papakyriakou, T.N., 2011. Carbonate system evolution at the Arctic Ocean surface during autumn freeze-up. J. Geophys. Res. Oceans 116, C00G04. doi:10.1029/2011JC007143

Millero, F.J., 1979. The thermodynamics of the carbonate system in seawater. Geochimica et Cosmochimica Acta 43(10), 1651-1661. https://doi.org/10.1016/0016-7037(79)90184-4

Mucci, A., 1983. The solubility of calcite and aragonite in seawater at various salinities, temperatures, and one atmosphere total pressure. American Journal of Science 283, 780-799.

Muckenhuber, S., Nilsen, F., Korosov, A., Sandven, S., 2016. Sea ice cover in Isfjorden and Hornsund, Svalbard (2000-2014) from remote sensing data. The Cryosphere 10, 149-158. https://doi.org/10.5194/tc-10-149-2016

Nilsen, F., Cottier, F., Skogseth, R., Mattsson, S., 2008. Fjord-shelf exchanges controlled by ice and brine production: The interannual variation of Atlantic Water in Isfjorden, Svalbard. Continental Shelf Research 28, 1838-1853. https://doi.org/10.1016/j.csr.2008.04.015

Nilsen, F., Skogseth, R., Vaardal-Lunde, J., Inall, M., 2016. A simple shelf circulation model: Intrusion of Atlantic Water on the West Spitsbergen Shelf. J. Phys. Oceanogr. 46(4), 1209–1230. https://doi.org/10.1175/JPO-D-15-0058.1

Omar, A., Johannessen, T., Bellerby, R.G.J., Olsen, A., Anderson, L.G., Kivimäe C., 2005. Sea ice and brine formation in Storfjorden: implications for the Arctic winter time air-sea CO_2 flux, in: Drange, H., Dokken, T., Furevik, T., Gerdes , R., Breger, W., (Eds.), The Nordic Seas: an integrated perspective. Geophysical Monograph 158, 177-187.

Pavlov, A.K., Tverberg, V., Ivanov, B.V., Nilsen, F., Falk-Petersen, S., Granskog, M.A. 2013. Warming of Atlantic Water in two west Spitsbergen fjords over the last century (1912-2009). Polar Research 32, 11206. https://dx.doi.org/10.3402/polar.v32i0.11206

Randelhoff, A., Fer, I., Sundfjord, A. 2017. Turbulent upper-ocean mixing affected by meltwater layers during Arctic summer. J. Phys. Oceanogr. 47, 835-853. https://doi.org/10.1175/JPO-D-16-0200.1

Redfield, A.C., Ketchum, B.H., Richards, F.A., 1963. The influence of organisms on the composition of sea-water, in: Hill, M.N., (Ed), The Sea: Ideas and Observations on the Progress in the Study of the Seas, vol. 2, pp. 26-77, Interscience, New York.

RFA (Rapid Flow Analyser) Methodology, 1989. Nitrate+Nitrite Nitrogen. A303-S170 Revision 6-89, College Station, TX: ALPKEM.

Rhein, M., Rintoul, S.R., Aoki, S., Campos, E., Chambers, D., Feely, R.A., Gulev, S., Johnson, G.C., Josey, S.A., Kostianoy, A., Mauritzen, C., Roemmich, D., Talley, L.D., Wang, F., 2013. Observations: Ocean, in: Stocker, T.F., Qin, D., Plattner, G.-K., Tignor, M., Allen, S.K., Boschung, J., Nauels, A., Xia, Y., Bex, V., Midgley, P.M. (Eds), Climate Change 2013: The Physical Science Basis. Contribution of Working Group I to the Fifth Assessment Report of the Intergovernmental Panel on Climate Change. Cambridge University Press, Cambridge, United Kingdom and New York, NY, USA.

Riley, J.P., Tongudai, M., 1967. The major cation/chlorinity ratios in sea water. Chemical Geology 2, 263-269.

Robbins, L.L., Wynn, J.G., Lisle, J.T., Yates, K.K., Knorr, P.O., Byrne, R.H., Liu, X., Patsavas, M.C., Azetsu-Scott, K., Takahashi, T., 2013. Baseline monitoring of the Wester Arctic Ocean estimates 20% of Canadian Basin surface waters are undersaturated with respect to aragonite. PLoS One 8(9), e73796. doi:10.1371/journal.pone.0073796

Rysgaard, S., Glud, R.N., Sejr, M.K., Bendtsen, J., Christensen, P.B., 2007. Inorganic carbon transport during sea ice growth and decay: A carbon pump in polar seas. J. Geophys. Res.112, C03016. doi:10.1029/2006JC003572

Rysgaard, S., Mortensen, J., Juul-Pedersen, T., Sørensen, L.L., Lennert, K., Søgaard, D.H., Arendt, K.E., Blicher, M.E., Sejr, M.K., Bendtsen, J., 2012. High air–sea CO_2 uptake rates in nearshore and shelf areas of Southern Greenland: Temporal and spatial variability. Mar. Chem. 128-129, 26-33. https://doi.org/10.1016/j.marchem.2011.11.002

Serreze, M.C., Francis, J. A., 2006. The Arctic amplification debate. Climatic Change 76, 241-264. doi: 10.1007/s10584-005-9017-y

Shadwick, E.H., Thomas, H., Chierici, M., Else, B., Fransson, A., Michel, C., Miller, L.A., Mucci, A., Niemi, A., Papakyriakou, T.N., Tremblay, J.-E., 2011. Seasonal variability of the organic carbon system in the Amundsen Gulf region of the southeastern Beaufort Sea. Limnol. Oceanogr. 56(1), 303-322.

Takahashi, T., Olafsson, J., Goddard, J.G., Chipman, D.W., Sutherland S.C., 1993. Seasonal variation of CO_2 and nutrients in the high latitude surface oceans: A comparative study. Global Biogeochem. Cycles 7(4), 843–878. https://doi.org/10.1029/93GB02263

Turk, D., Bedard, J.M., Burt, W.J., Vagle, S., Thomas, H., Azetsu-Scott, K., McGillis, W.R., Iverson, S.J., Wallace, D.W.R., 2016. Inorganic carbon in a high latitude estuary-fjord system in Canada's eastern Arctic. Eustarine, Coastal, and Shelf Science 178, 137-147. http://dx.doi.org/10.1016/j.ecss.2016.06.006

van Heuven, S., Pierrot, D., Rae, J.W.B., Lewis, E., Wallace, D.W.R., 2011. MATLAB program developed for CO2 system calculations. ORNL/CDIAC-105b, Carbon Dioxide Information Analysis Center, Oak Ridge National Laboratory, Oak Ridge, Tennessee. doi: 10.3334/CDIAC/otg.CO2SYS_MATLAB_v1.1

Wanninkhof, R., 2014. Relationship between wind speed and gas exchange over the ocean revisited. Limnol. Oceanogr. Methods 12(6), 351–362. https://doi.org/10.4319/lom.2014.12.351

Weiss, R.F., 1974. Carbon dioxide in water and seawater: the solubility of a non-ideal gas. Mar. Chem. 2(3), 203–205. https://doi.org/10.1016/0304-4203(74)90015-2

World Meteorological Organization (WMO), 2014. Guide to Meteorological Instruments and Methods of Observation (WMO-No 8). Geneva, Switzerland.

Woosley, R.J., Millero, F.J., Takahashi, T., 2017. Internal consistency of the inorganic carbon system in the Arctic Ocean. Limnol. Oceanogr. Methods 15(10), 887-896. https://doi.org/10.1002/lom3.10208

Yamamoto-Kawai, M., McLaughlin, F.A., Carmack, E.C., Nishino, S., Shimada, K., 2009. Aragonite Undersaturation in the Arctic Ocean: Effects of Ocean Acidification and Sea Ice Melt. Science 326, 1098-1100.

Zeebe, R.E., Wolf-Gladrow, D.A., 2001. CO_2 in seawater: Equilibrium, kinetics, isotopes. Elsevier Oceanography Series 65, pp. 1-84.

Ziaja, W., 2005. Response of the Nordenskiöld Land (Spitsbergen) glaciers Grumantbreen, Håbergbreen and Dryadbreen to the climate warming after the Little Ice Age. Annals of Glaciology 42, 189-194.